

AperTO - Archivio Istituzionale Open Access dell'Università di Torino

**Cyclic nigerosyl-1,6-nigerose-based nanosponges: An innovative pH and time-controlled nanocarrier for improving cancer treatment**

**This is a pre print version of the following article:**

*Original Citation:*

*Availability:*

This version is available <http://hdl.handle.net/2318/1676447> since 2020-02-21T13:37:11Z

*Published version:*

DOI:10.1016/j.carbpol.2018.04.027

*Terms of use:*

Open Access

Anyone can freely access the full text of works made available as "Open Access". Works made available under a Creative Commons license can be used according to the terms and conditions of said license. Use of all other works requires consent of the right holder (author or publisher) if not exempted from copyright protection by the applicable law.

(Article begins on next page)

1 **Cyclic nigerosyl-1,6-nigerose-based nanosponges: an innovative pH and time-controlled**  
2 **nanocarrier for improving cancer treatment**

3  
4 F. Caldera<sup>1\*</sup>, M. Argenziano<sup>2\*</sup>, F. Trotta<sup>1</sup>, C. Dianzani<sup>2</sup>, L. Gigliotti<sup>3</sup>, M. Tannous<sup>1</sup>, L. Pastero<sup>4</sup>, D.  
5 Aquilano<sup>4</sup>, T. Nishimoto<sup>5</sup>, T. Higashiyama<sup>6</sup>, R. Cavalli<sup>2</sup>

6  
7  
8  
9 <sup>1</sup>Dipartimento di Chimica – Università di Torino. Via P. Giuria 7, 10125 Torino – Italy

10 <sup>2</sup>Dipartimento di Scienza e Tecnologia del Farmaco – Università di Torino. Via P. Giuria 9, 10125  
11 Torino – Italy

12 <sup>3</sup> Dipartimento di Scienze della Salute, UPO, via Solaroli 17, 28100 Novara - Italy

13 <sup>4</sup>Dipartimento di Scienze della Terra, Università di Torino. Via V. Caluso 35, 10125 Torino – Italy

14 <sup>5</sup>Division Manager New Material Development Division R&D Center Hayashibara Co., Ltd. 675-1  
15 Fujisaki, Naka-ku, Okayama 702-8006, Japan

16 <sup>6</sup>NAGASE (EUROPA) GmbH/ Hayashibara - Immermannstrasse 65c, 40210 Düsseldorf, Germany

17  
18  
19  
20  
21  
22 \* Equal contribution to the work.

23  
24 **Corresponding author:**

25 Roberta Cavalli,

26 Department of Drug Science and Technology,

27 University of Turin

28 Via Pietro Giuria 9,

29 10125 Turin, Italy

30 Phone: +390116707190

31 Fax: +390116707687

32 e-mail: roberta.cavalli@unito.it

33 **Abstract**

34 The design and structural optimisation of a novel polysaccharide-based nanomaterial for the  
35 controlled and sustained release of doxorubicin are here reported. A cross-linked polymer was  
36 obtained by reacting a tetraglucose, named cyclic nigerosyl-1-6-nigerose (CNN), with pyromellitic  
37 dianhydride. The cross-linking reaction formed solid nanoparticles, named nanosponges, able to  
38 swell as a function of the pH. Nanoparticle sizes were reduced using High Pressure  
39 Homogenization, to obtain uniform nanosuspensions. Doxorubicin was incorporated into the CNN-  
40 nanosponges in a good extent. DSC and solid state NMR analyses proved the drug interaction with  
41 the polymer matrix. *In vitro* studies demonstrated pH-dependent slow and prolonged release  
42 kinetics of the drug from the nanoformulation. Doxorubicin-loaded CNN-nanosponges were easily  
43 internalized in A2780 cell line. They might considered an intracellular doxorubicin reservoir, able  
44 to slowly release the drug over time. CNN-nanosponges may be promising biocompatible  
45 nanocarriers for the sustained delivery of doxorubicin with potential localised application in cancer  
46 treatments.

47

48

49 **Keywords:** CNN, nigerose, nanosponges, doxorubicin, sustained release

50

## 51 **1. Introduction**

52 Controlled and sustained release delivery systems of drugs may open up new avenues in  
53 nanotherapeutic fields to overcome some drug limitations, with spatial and time-controlled release  
54 kinetics (Arpicco et al., 2016, Prasad et al., 2018). A number of these formulations have used  
55 nanoscaled carriers encapsulation. Indeed, drug delivery system-based nanoparticles, able to store  
56 and release molecules for an extended period of time (weeks or months) and as a function of an  
57 external stimulus, can play a key role in developing safer and more effective nanomedicines (Mura,  
58 Nicolas & Couvreur, 2013). The use of nanocarriers allows for the modulation and modification of  
59 the physico-chemical properties of drugs, producing improved pharmacokinetics and bio-  
60 distribution profiles (Hamidi, Azadi, Rafiei & Ashrafi, 2013). Various biodegradable and  
61 biocompatible polymer systems could be used as interesting advanced controlled-release systems  
62 for bioactive molecules (Duchene, Cavalli & Gref, 2016). Polymer nanoparticles are easy to  
63 produce with improved stability and more control over drug release (Jaimes-Aguirre, et al., 2016).  
64 Indeed, drug release kinetics can be precisely controlled by the physico-chemical properties of the  
65 polymer, such as molecular weight, porosity, hydrophobicity and crystallinity (Bhattacharjee et al.,  
66 2016). Moreover, the presence of specific moiety in the polymer structure, responsive to external  
67 stimuli, i.e. dissociable carboxylic groups or redox reactive groups, may facilitate localised drug  
68 delivery (Liu, Yang & Urban, 2017).

69 Notably, prolonged-release polymer nanoparticles can reduce the frequency of administration of  
70 drugs, particularly those with a short half-life, stabilise drug absorption, decrease the occurrence of  
71 adverse side effects and improve patients' adherence to therapy (Natarajan, Nugraha, Ng &  
72 Venkatraman, 2014). In particular, poly(lactic-co-glycolic acid (PLGA), a biodegradable polyester  
73 approved for human use, has been extensively studied to obtain sustained release nanovectors.  
74 Much attention in research has been focused on designing PLGA nanosystems for the controlled  
75 delivery of anticancer drugs (Dinarvand, Sepehri, Manoochehri, Rouhani & Atyabi, 2011, Khan et  
76 al., 2016). A number of PLGA nanoparticles were studied for doxorubicin, tuning the formulation  
77 design to obtain prolonged release kinetics. Doxorubicin-loaded PLGA nanoparticles with the  
78 surface modified with poly(L- $\gamma$ -glutamic acid) ( $\gamma$ -PGA) and finally conjugated with folic acid  
79 showed a release profile lasting over 7 days (Jaimes-Aguirre et al., 2017).

80 Cross-linked polymer nanoparticles represent an alternative formulation approach. Recently,  
81 cyclodextrin-based nanosponges, hyper cross-linked cyclodextrin polymers, with sizes in the  
82 nanometer order of magnitude, have been designed as a drug delivery nanosystem (Trotta, Zanetti  
83 & Cavalli, 2012, Liang et al., 2013, Trotta, Dianzani, Caldera, Mognetti & Cavalli, 2014, Caldera,

84 Tannous, Cavalli, Zanetti & Trotta, 2017, Liang et al., 2017, Sherje, Dravyakar, Kadam, Jadhav,  
85 2017). Cyclodextrins are a class of cyclic glucopyranose oligomers with a characteristic toroidal  
86 shape that forms a well-defined truncated cone-shaped lipophilic cavity. Cyclodextrins are able to  
87 include compounds whose geometry and polarity are compatible with that of their cavity  
88 (Muankaew & Loftsson, 2018). Cyclodextrin-based nanosponges exhibited a superior inclusion  
89 capability than parent cyclodextrins. Indeed, they were able to incorporate many types of molecules,  
90 such as small molecules, macromolecules and gases (Trotta et al., 2014, Swaminathan et al., 2010a,  
91 Cavalli et al., 2010). The loaded molecules are generally delivered with a slow and prolonged  
92 release profile, according to the nanoparticle network structure. Indeed, the release can be  
93 influenced by the cross-linking ratio and the nature of the polymer mesh to obtain a sustained and  
94 controlled delivery (Swaminathan et al., 2010b, Torne, Ansari, Vavia, Trotta & Cavalli, 2010, Daga  
95 et al., 2016, Gigliotti et al., 2017). The incorporation and storage capability is strongly affected by  
96 the polymer nanostructure, as well as the presence of many cyclodextrin cavities able to cooperate.  
97 To load hydrophilic or charged molecules, modifications of nanosponges were devised.  
98 Interestingly, the introduction of charged groups either in the nanostructure or on the surface of  
99 nanosponges enabled the production of further interaction sites for loading dissociable drugs  
100 (Lembo et al., 2013, Bastiancich et al., 2014). Based on these premises and to expand the possibility  
101 of controlling the release, another cyclic oligosaccharide. i.e. a tetraglucose, was selected as a  
102 building block of new nanosponges, in place of cyclodextrins (Wei, et al. 2015). Intriguingly, cyclic  
103 nigerosyl-1-6-nigerose, (CNN) is a non-reducing cyclic tetrasaccharide with a unique structure  
104 consisting of four D-glucopyranosyl molecules connected by alternate  $\alpha$ -(1-3) and  $\alpha$ -(1-6)  
105 glycosidic bonds (Fig. 1A). CNN differs from cyclodextrin not only due to its number of glucose  
106 units (4) and type of glucosidic bond, but also due to the arrangement of the hydroxyl groups.  
107 Namely, two of them are oriented toward the inner cavity of CNN, making it quite polar.  
108 This cyclic tetrasaccharide is obtained from hydrolysed starch by the action of a mixture of  
109 enzymes (Nishimoto et al., 2002, Aga et al., 2003). Cyclotetraglucose occurs naturally in sake lees  
110 (i.e., the sediment that forms during rice wine production), in sake itself and in food-grade starch  
111 (e.g., tapioca starch, cornstarch) (Watanabe et al., 2004). The industrial manufacturing production  
112 is done by Hayashibara (Japan). This tetraglucose is a white crystalline powder which is safe and  
113 stable to temperature, while at alkaline pH values a slow degradation was observed (Weissenfeld,  
114 2005). The capacity to interact as such with various molecules was studied. The complexation of  
115 some aromatic compounds with CNN was investigated, showing the formation of guest-CN  
116 complexes with vanillin, cinnamaldehyde and eugenol (Ishikawa, Kuwano, Chaen & Matsumoto,

117 2009). Moreover, CNN have been used for powdering tocopherol, vitamin D and EPA (Oku et al.,  
118 2007).

119 This work aims at exploiting the CNN unit as a monomer for the synthesis of new cross-linked  
120 polymers, called CNN-nanosponges (CNN-NS). To obtain the CNN-based polymer, a synthetic  
121 protocol was tuned, selecting pyromellitic dianhydride (PMDA) as a cross-linker (Figure 1B).

122 Firstly, three types of CNN-NS will be considered varying the molar ratio between CNN and  
123 pyromellitic dianhydride (i.e. 1:2, 1:4, 1:6 ratios, respectively) to optimise the nanostructure for  
124 drug delivery. Their physico-chemical characterisation will be studied and the drug loading  
125 capability will be investigated using doxorubicin as the model molecule. Finally, the *in vitro*  
126 biological behaviour of doxorubicin-loaded CNN-NS will be evaluated.

127

128 **2. Material and methods**

129

130 *2.1 Materials*

131 Cyclic nigerosyl-1-6-nigerose (CNN) was received as a kind gift from Hayashibara (Japan).  
132 Doxorubicin hydrochloride and pyromellitic dianhydride (PMDA) were purchased from Sigma.  
133 Solvents and reagents, unless otherwise indicated, were analytical-grade commercial products, used  
134 as received.

135

136 *2.2 CNN-nanosponges synthesis*

137 The quantities of chemicals used for the synthesis of the three NS are listed in table 1. In summary,  
138 4.886 g of CNN, desiccated in an oven at 100°C up to constant weight, were solubilised in 20 mL  
139 of dimethyl sulfoxide (DMSO) at room temperature. Subsequently, 5 mL of triethylamine (Et<sub>3</sub>N)  
140 and, after a few minutes, the correct amount of pyromellitic dianhydride were added. The solution  
141 was vigorously stirred until gelation point was reached. The obtained monolithic block was then  
142 crushed, recovered by vacuum filtration, washed with an excess of deionised water and rinsed with  
143 acetone. After drying at room temperature, the powder was collected and further purified through  
144 Soxhlet extraction for 24 h with acetone. The scheme of the CNN-NS synthesis reaction is shown in  
145 figure 1B.

146

147 **Table 1.** Quantities of chemicals used in the synthesis of the three types of CNN-NS

148

	DMSO		CNN		Et <sub>3</sub> N		PMDA		PMDA/CNN
	(mL)	(mmol)	(g)	(mmol)	(mL)	(mmol)	(g)	(mmol)	molar ratio
<b>CNN-NS (1:2)</b>	20.0	281.6	4.886	7.534	5.0	35.9	3.286	15.067	2
<b>CNN-NS (1:4)</b>	20.0	281.6	4.886	7.534	5.0	35.9	6.573	30.134	4
<b>CNN-NS (1:6)</b>	20.0	281.6	4.886	7.534	5.0	35.9	9.859	45.202	6

149

150

151

152

153 *2.3 Swelling degree evaluation*

154 Dry CNN-NS specimens of known weights were immersed in buffer solutions with different pH  
155 values at room temperature (i.e. pH 2.0, pH 4.0, pH 6.0 and pH 7.4 disodium hydrogen  
156 phosphate/phosphoric acid buffer). At pre-determined time intervals, the swollen nanosponges were  
157 removed from the buffer, blotted with filter paper to absorb the excess surface solution and  
158 immediately weighed. The procedure was repeated until there was no further weight increase. The  
159 swelling degree (SD) was then calculated as follows:

$$SD = \frac{(W_t - W_d)}{W_d}$$

160 where  $W_t$  is the weight of the swollen nanosponges and  $W_d$  is the weight of the nanosponges in the  
161 dry state. All experiments were performed in triplicate.

162

163 *2.4 X-ray powder diffraction (XRPD) analysis*

164 To characterise the nanosponges, we carried out a detailed XRPD analysis using a Siemens D5000  
165 diffractometer (Cu K $\alpha$ 1, Bragg-Brentano geometry, sequential collection between 2.5° and 60° 2 $\theta$ ).  
166 The diffraction patterns were analysed using Fityk software (Wojdyr, 2010).

167

168 *2.5 DSC analysis*

169 Differential Scanning Calorimetry (DSC) was carried out by means of a Perkin Elmer DSC/7  
170 differential scanning calorimeter (Perkin-Elmer, CT-USA) equipped with a TAC 7 /DX instrument  
171 controller. The instrument was calibrated with indium for melting point and heat of fusion. A  
172 heating rate of 10°C/min was employed in the 25-250°C temperature range. Standard aluminium  
173 sample pans (Perkin-Elmer) were used; an empty pan was used as a reference standard. Analyses  
174 were performed in triplicate on 3 mg samples under nitrogen purge.

175

176 *2.6 Preparation of doxorubicin-loaded CNN-nanosponges (1:4)*

177 An aqueous suspension of the CNN-NS(1:4) at the concentration of 10 mg/ml was prepared. A pre-  
178 homogenisation was carried out for 10 min of Ultraturrax (Ika, Germany) at 24,000 rpm. The  
179 aqueous suspension was then transferred into a high pressure homogeniser (HPH) (Emulsiflex C5,  
180 Avestin, USA) and subjected to homogenisation. The protocol tuned consists of 5 cycles at 5,000  
181 psi for 5 min, 12 cycles at 7,000 for 90 min. The obtained aqueous nanosuspension was purified by  
182 dialysis and stored at 4°C. An aqueous solution of doxorubicine (2 mg/ml) was incubated at room  
183 temperature with the CNN nanosuspension under mild stirring for 12 hours. Subsequently, a



184 dialysis step was performed to eliminate the unloaded doxorubicin. For cell experiments the  
185 nanosuspension was prepared in NaCl 0.9% w/v aqueous solution.

186

### 187 *2.7 Quantitative determination of doxorubicin*

188 The quantitative determination of doxorubicin was carried out by a HPLC system consisting of a  
189 pump (LC-9A PUMP C, Shimadzu, Japan) equipped with a fluorescence detector (Chrompack,  
190 Japan). Analyses were performed using an Agilent TC C<sub>18</sub> column (250 mm × 4.6 mm, 5 μm). The  
191 mobile phase was a mixture of 0.01 M KH<sub>2</sub>PO<sub>4</sub> (pH 1.4), acetonitrile and methanol (65:25:10  
192 v/v/v), degassed and pumped through the column at a flow rate of 1 ml/min. The column effluent  
193 was monitored at excitation and emission wavelengths of 480 and 560 nm, respectively. The  
194 external standard method was used to calculate the drug concentration. For this purpose, 1 mg of  
195 doxorubicin was weighed, placed in a volumetric flask, and dissolved in water to obtain a stock  
196 standard solution. This solution was then diluted using the mobile phase, providing a series of  
197 calibration solutions, subsequently injected into the HPLC system. The linear calibration curve was  
198 obtained over the concentration range of 0.025–2.5 μg/ml with a regression coefficient of 0.999.

199

### 200 *2.8 Determination of doxorubicin encapsulation efficiency*

201 A 10 mg/mL aqueous suspension of the freeze-dried loaded nanosponges was prepared using  
202 filtered water and doxorubicin extracted by sonication for 5 minutes at room temperature. After  
203 centrifugation, the drug concentration in the supernatant was determined by the HPLC method  
204 previously described. Encapsulation efficiency and drug loading were then calculated using the  
205 calibration curve.

206

### 207 *2.9 Size, polydispersity index and zeta potential values*

208 CNN-NS sizes and polydispersity indices were measured by dynamic light scattering using a 90  
209 Plus particle sizer (Brookhaven Instruments Corporation, USA) equipped with MAS OPTION  
210 particle sizing software. The measurements were made at a fixed angle of 90° for all samples,  
211 which were suitably diluted with filtered and distilled water for every measurement. The zeta  
212 potential measurements were also taken using an additional electrode in the same instrument. For  
213 zeta potential determination, samples of the three formulations were diluted with 0.1 mM KCl and  
214 placed in the electrophoretic cell, where an electric field of about 15 V/cm was applied.

215

### 216 *2.10 Solid state NMR analysis*

217 Solid state NMR spectra were acquired using a Jeol ECZR 600 instrument, operating at 600.17 and  
218 150.91 MHz for <sup>1</sup>H and <sup>13</sup>C nuclei, respectively. Powder samples were packed into cylindrical  
219 zirconia rotors with a 3.2 mm OD and a 60 μL volume. A certain amount of sample was collected  
220 from each batch and used without further preparations to fill the rotor. <sup>13</sup>C CPMAS spectra were  
221 acquired at a spinning rate of 20 kHz using a ramp cross-polarisation pulse sequence with a contact  
222 time of 3.5 ms, a 90° <sup>1</sup>H pulse of 2.189 μs, (optimised) recycle delays of 3.5 s (doxorubicin), 1.9s  
223 (blank CNN-NS (1:4)) and 0.4s (doxorubicin-loaded CNN-NS(1:4)) and a number of scans  
224 included between 2000 and 10000, depending on the sample. For every spectrum a two pulse phase  
225 modulation (TPPM) decoupling scheme was used, with a radiofrequency field of 108.5 kHz. The  
226 chemical shift scale was calibrated through the methylenic signal of external standard glycine (at  
227 43.7 ppm).

228

### 229 *2.11 Morphology analysis*

230 Transmission electron microscopy (TEM) was used to evaluate particle shape and morphology. A  
231 Philips CM 10 transmission electron microscope was used and the particle size was measured using  
232 the NIH image software. The nanosponge suspensions were sprayed on Formwar-coated copper  
233 grid and air-dried before observation.

234 Scanning electron microscopy (SEM) was used to evaluate the morphology of the CNN-NS  
235 formulations using a JEOL JSM IT300LV (EHT 20 kV, working distance 10 mm). The  
236 nanosponges were positioned on a conductive sample holder and sputtered with graphite to assure  
237 the conductivity of the sample.

238

### 239 *2.12 ATR FTIR analysis*

240 ATR FTIR analysis was applied to doxorubicin-loaded CNN-NS, free doxorubicin and plain CNN-  
241 NS using a Perkin Elmer 2000 instrument. The spectra were recorded between 400 and 4000 cm<sup>-1</sup>.

242

### 243 *2.13 Stability evaluation of CNN-nanosponges*

244 The physical stability of CNN-NS was evaluated over time, determining size, surface charge and  
245 doxorubicin loading, as previously described. This thermal stability of CNN-NS can allow for  
246 sterilisation by autoclaving for cell experiments.

247

### 248 *2.14 In vitro release of doxorubicin from CNN-nanosponges (1:4)*

249 The *in vitro* release was carried out using multi-compartment rotating cells with a dialysis  
250 membrane (Sartorius, cut off 12,000 Da). The donor phase consisted of nanosponge formulation  
251 containing a fixed amount of doxorubicin in phosphate buffer at pH 7.4 (1 ml). The receiving phase  
252 consisted of phosphate buffer, pH 7.4 or pH 5.5 added with 0.5% w/v sodium lauryl sulphate (1 ml)  
253 to maintain proper sink conditions. The receiving phase was completely withdrawn and replaced  
254 with fresh medium after fixed time intervals, suitably diluted and analysed using the HPLC method  
255 described above.

256

## 257 *2.15 Biological assays*

258

### 259 *2.15.1 Haemolytic activity of CNN-nanosponges*

260 CNN-NS (10 mg/mL) were incubated at 37°C for 90 minutes with 1 ml of diluted blood. Freshly  
261 prepared PBS (pH 7.4) was used for all dilution purposes. After incubation, blood-containing  
262 suspensions were centrifuged at 2,000 rpm for 10 min to separate the plasma. The amount of  
263 haemoglobin released due to haemolysis was measured spectrophotometrically at 543 nm (Du 730,  
264 Beckman). The haemolytic activity was calculated with reference to blank and complete  
265 haemolysed samples (induced by the addition of ammonium sulphate 20% w/v). Optical  
266 microscopy was also used to see if there were any abnormalities in the blood cells after incubation.  
267 The observations were made with reference to the blank diluted blood. No changes in red blood cell  
268 morphology were detected.

269

### 270 *2.15.2 In vitro cytotoxicity determination*

271 The ovarian cell line, A2780, was obtained from the American Type Culture Collection (Rockville,  
272 MD, USA). The cells were grown as a monolayer culture in RPMI 1640 medium supplemented  
273 with 10% heat-inactivated fetal calf serum (FCS), 2 mmol/l L-glutamine and  
274 penicillin/streptomycin (100 units/ml), at 37°C in 5% CO<sub>2</sub> humidified atmosphere.

275

### 276 *2.15.3 Colony-forming assay*

277 Cells (1,000 per well) were seeded into six-well plates and treated with the compounds. The  
278 medium was changed after 72 h and cells were cultured for an additional 10 days without any drug.  
279 Subsequently, the cells were fixed and stained with a solution of 80% crystal violet (Sigma-Aldrich)  
280 and 20% methanol for 30 min. The cells were then perfectly washed and 30% acetic acid was added

281 to induce a complete dissolution of the crystal violet. Absorbance was recorded at 595 nm by a 96-  
282 well-plate ELISA reader. Five different experiments were performed.

283

#### 284 *2.15.4 In vitro uptake study*

285  $5 \times 10^4$  cell/well of A2780 cells were seeded in 24-well plates in 1 ml of culture medium and treated  
286 with  $10^{-7}$  M free Doxorubicin or CNN Doxorubicin. 48 h (T48) later the cells cultured on the  
287 coverslips were rinsed three times with cold PBS and fixed with 75% ethanol for 30 min at 4°C and  
288 the coverslips were inverted and mounted on glass slides. The nuclei were stained with 4',6'-  
289 diamidino-2-phenylindole (DAPI 1 mg·mL<sup>-1</sup>; Sigma-Aldrich, Saint Louis, MO, USA). The slides  
290 were analysed by confocal laser scanning microscopy (CLSM) using a Leica DMIRE2 confocal  
291 fluorescence microscope (Leica Microsystems AG, Wetzlar, Germany) equipped with Leica  
292 Confocal Software v. 2.61.

293

#### 294 *2.16. Statistical analysis*

295 Data are shown as mean  $\pm$  SEM. Statistical analyses were performed with GraphPad Prism 3.0  
296 software (La Jolla, CA, USA) using one-way ANOVA and Dunnett's test. Values of  $P < 0.05$  were  
297 considered statistically significant.

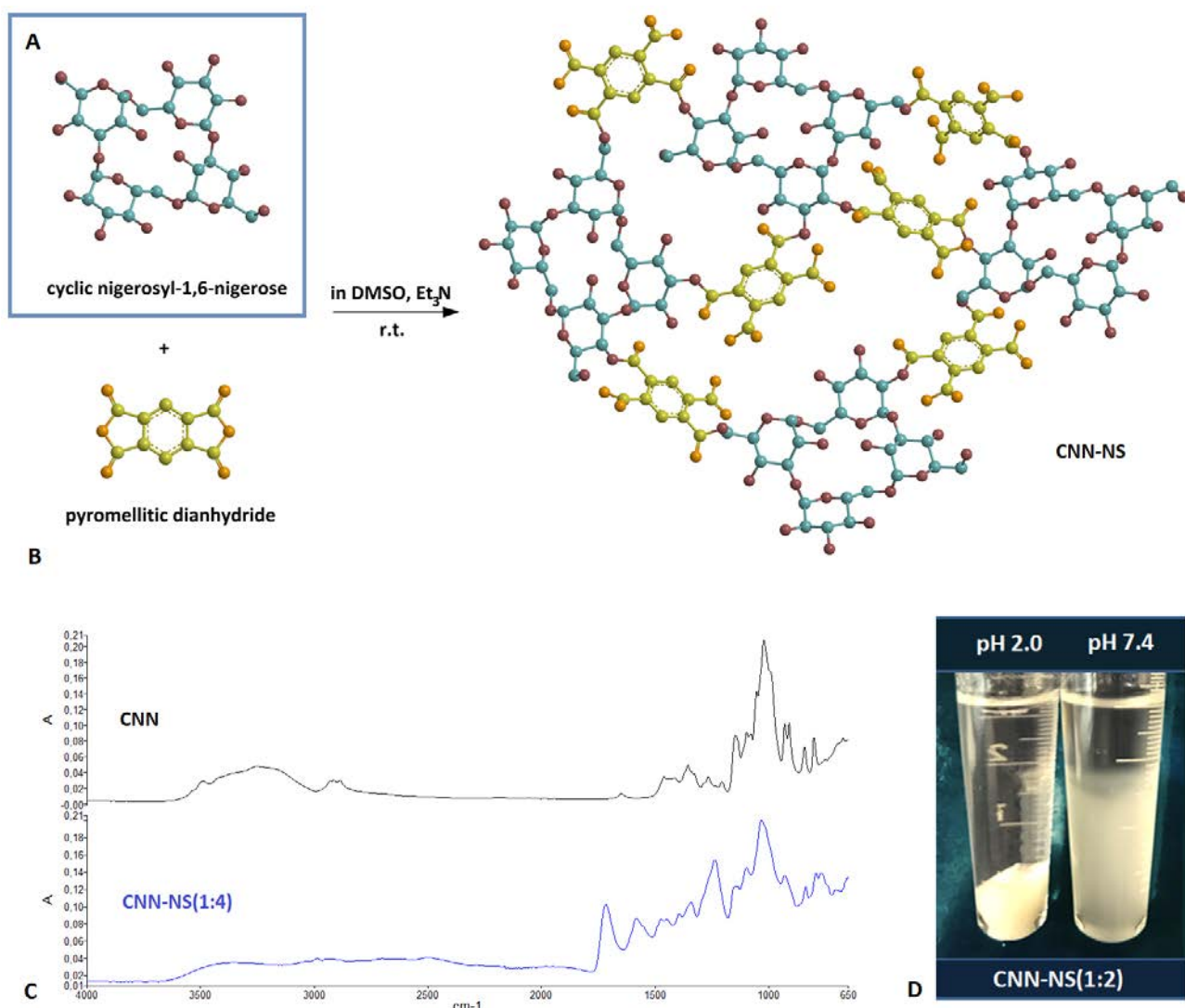
298

299

300 **3. Results and Discussion**

301 One strategy to improve the therapeutic effectiveness and to reduce the side effects of anticancer  
302 drugs on healthy cells is to improve local drug concentrations at the disease tissues. Biocompatible  
303 nanoparticles containing drugs can provide a site-specific delivery of anticancer drugs in a  
304 controlled and sustained manner improving the safety profile (Brigger, Dubernet & Couvreur,  
305 2002). Nanoscaled delivery systems can carry loaded drugs to the tumour site through the  
306 bloodstream, taking advantage of the enhanced permeability and retention (EPR) effect, due to the  
307 defective vascular architecture of the tumour (Fang, Nakamura & Maeda, 2011, Maeda, Nakamura  
308 & Fang, 2013). Stimuli-responsive polymer nanoparticles can allow more precise and controlled  
309 release behaviour (Cheng, Meng, Deng, Klok & Zhong, 2013). Based upon these concepts, a new  
310 nanodelivery system has been developed, using a biocompatible tetraglucose, i.e. cyclic nigerosyl-  
311 1-6-nigerose (CNN), as an innovative building block. Solid cross-linked polymer nanoparticles,  
312 named cyclic nigerosyl-1-6-nigerose based nanosponges (CNN-NS) were prepared, by the reaction  
313 of CNN with pyromellitic dianhydride, to obtain pH responsiveness. Figure 1B reports the schematic  
314 representation of the CNN-NS synthesis reaction.

315



316

317 **Figure 1.** A) Chemical structure of cyclotetraglucose (CNN) B) Scheme of the CNN-NS  
 318 synthesis reaction C) ATR-FTIR spectra of CNN and CNN-NS D) Swelling capacity of CNN-NS  
 319 (1:2) as a function of pH values (pH 2 and 7.4).

320

321 PMDA was selected, among several cross-linkers, for its high reactivity towards hydroxyl groups,  
 322 which allows fast reactions with high yields and because of the interactions that carboxylic groups  
 323 of pyromellitic bridges may establish with polar moieties of drugs (i.e. -COOH, -NH<sub>2</sub>, -OH  
 324 groups). These interactions might contribute to high encapsulation efficiency and slow release  
 325 kinetics. Moreover, the high content of carboxylic groups, introduced by PMDA, confers a pH-  
 326 sensitive character to CNN-NS, which may be profitably exploited to modulate the release of  
 327 loaded drugs. The presence of the cross-linked network was confirmed by FTIR analysis. Indeed,  
 328 the absorption band typical of carboxylate groups appeared in the FTIR-ATR spectrum of CNN-NS  
 329 at 1580 cm<sup>-1</sup>, along with other signals deriving from pyromellitic units (i.e. C=O stretching in

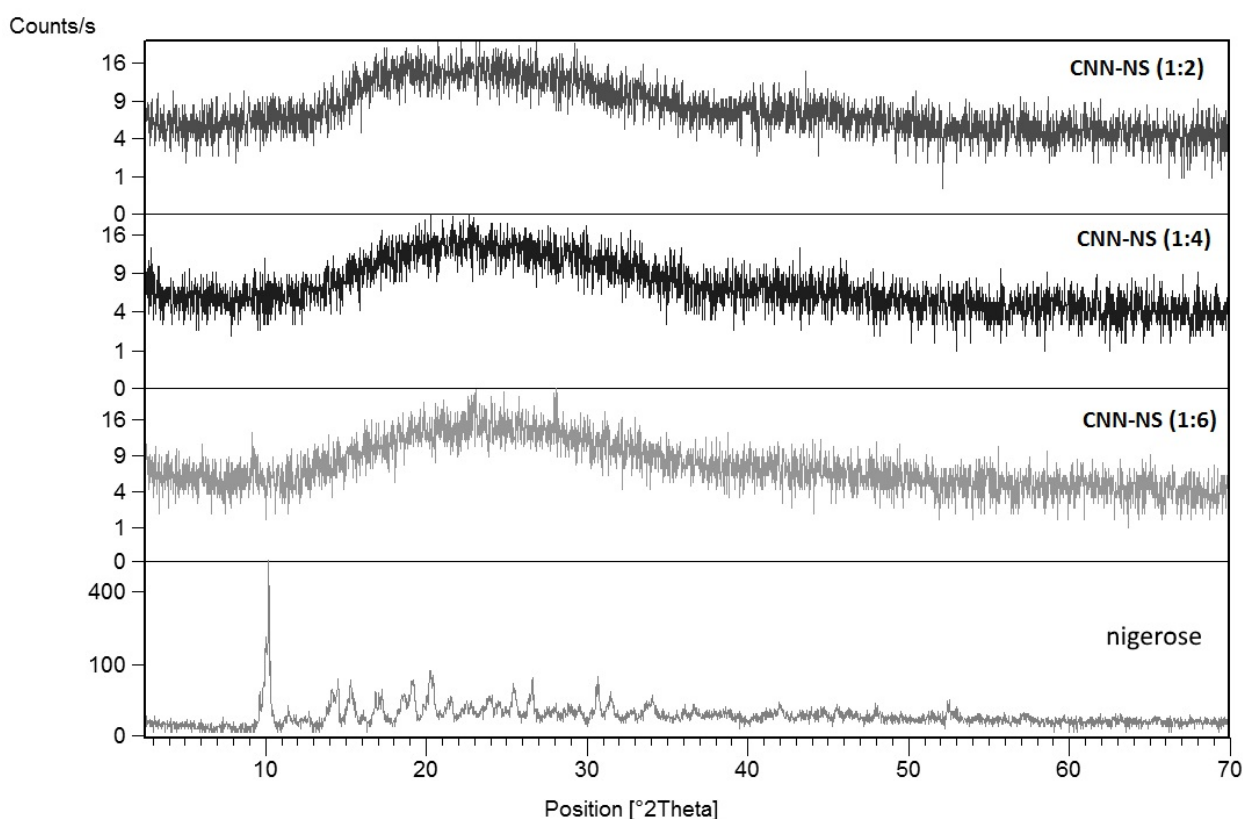
330 carboxylic groups at  $1720\text{ cm}^{-1}$  and C-O stretching in ester groups at  $1240\text{ cm}^{-1}$ , approximately) was  
331 not detected in the spectrum of pristine CNN (figure 1C).

332 The synthetic process is one-step, cost-effective and its repeatability and scalability have been  
333 confirmed. After synthesis, the solid CNN-NS underwent to the HPH step to decrease the  
334 nanoparticle dimensions and to produce smaller sizes and more uniform distribution. Indeed, the  
335 CNN-NS sizes were reduced reaching sizes lower than 400 nm.

336 Here, the optimisation and *in vitro* characterisation of this new tetraglucose-based nanodelivery  
337 system are reported. Firstly, the effect of the three different CNN cross-linker ratios (i.e. 1:2, 1:4  
338 and 1:6) on the nanostructure and physico-chemical properties was investigated to characterise the  
339 three products. All the obtained CNN-NS are amorphous solids, although CNN as such is markedly  
340 crystalline. Figure 2 shows the XRPD diagrams of the three types of CNN-NS compared with that  
341 of nigerose.

342

343



344

345 **Figure 2.** X-ray powder diffraction patterns of the CNN-NS obtained by reacting the CNN with  
346 variable concentrations of pyromellitic dianhydride (1:2, 1:4, 1:6 respectively) compared with the  
347 XRPD of the nigerose (bottom).

348

349 Despite the high degree of crystallinity displayed by nigerose, CNN-NS highlight their amorphous  
350 behaviour, shown by the broad bump in the range 10-40 °2 $\theta$ .

351 The amorphous nature was confirmed by DSC analyses. No peaks correlated to thermal changes  
352 were observed until 250°C (data not shown).

353 CNN-NS were easily able to absorb water and their swelling capacity was investigated as a function  
354 of the pH value of the external environment.

355 The three types of CNN-NS showed a marked swelling capacity related to the cross-linking degree,  
356 which remarkably depends on the pH value (Table 2).

357 Interestingly, CNN-NS were pH sensitive due to the presence of dissociable carboxylic groups in  
358 the polymer matrices. In particular, the swelling degree of the three types of nanosponges linearly  
359 increased from pH 2.0 to pH 7.4.

360 Table 2 reports the swelling degree of the two nanosponges as a function of pH values of the  
361 external medium.

362

363 **Table 2.** Swelling degree of CNN-NS as a function of pH values of the external medium.

Sample	Swelling degree (%)			
	pH 2.0	pH 4.0	pH 6.0	pH 7.4
CNN-NS (1:2)	562	680	765	820
CNN-NS (1:4)	124	215	307	415
CNN-NS (1:6)	88	206	248	392

364

365 It can be seen that CNN-NS (1:2) demonstrated a higher water uptake capability at all the pH values  
366 than those of the other two CNN-NS with higher degrees of cross-linking (Figure 1D).

367 Indeed, the lower the cross-linking degree, the higher the observed swelling. Interestingly, CNN-NS  
368 can be considered a quasi super-absorbent material, that was able to retain more than 800 wt% of  
369 water at room temperature and pH 7.4.



370 In this work, doxorubicin was selected as a model drug. Doxorubicin is one of the most common  
371 anticancer drug, but it suffers of severe side effects and multidrug resistance. Therefore a  
372 nanoformulation to improve its pharmacokinetics and biodistribution would be valuable.  
373 Preliminary explorative experiments proved that CNN-NS (1:4) were the most suitable for loading  
374 and storing doxorubicin. As a consequence, this type of CNN-NS was selected for further  
375 investigation and characterization with the drug.

376 Table 3 reports the physico-chemical characterization of doxorubicin-loaded and unloaded CNN-  
377 NS (1:4).

378

379

380

381

382

383

384

385 **Table 3.** Physico-chemical characterization of blank and doxorubicin-loaded CNN-NS

386

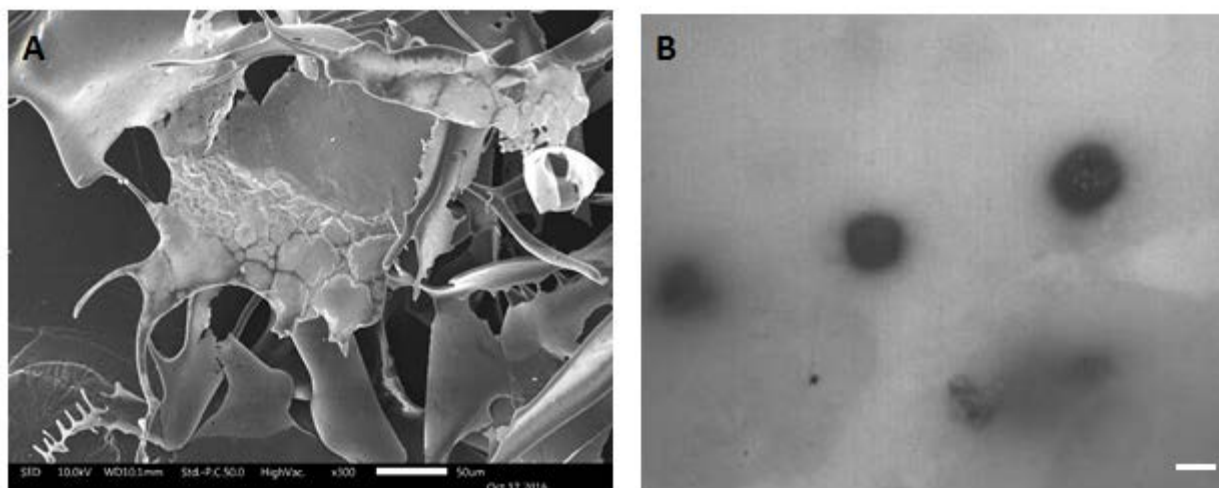
387

	<b>CNN-NS (1:4) (unloaded)</b>	<b>Doxorubicin-loaded CNN-NS (1:4)</b>
Average diameter $\pm$ SD (nm)	355.6 $\pm$ 27.3	360.8 $\pm$ 15.6
PDI	0.20 $\pm$ 0.02	0.19 $\pm$ 0.03
PZ $\pm$ SD (mV)	- 30.2 $\pm$ 4.55	- 29.2 $\pm$ 5.29
Loading capacity (%)	-	15.5
Encapsulation efficiency (%)	-	95.1

388

389 Doxorubicin encapsulation in CNN-NS did not require high-energy processes or solvent use  
390 preserving the drug from potential degradation. Interestingly, it is incorporated by incubation at  
391 room temperature under mild stirring. Doxorubicin is a hydrophilic drug with a good aqueous  
392 solubility (10 mg/ml). The hydrophilicity of the polymer mesh and probably the polarity of the  
393 CNN cavity provide drug encapsulation with high efficiency. The polymer network should play the

394 key role in the drug incorporation. Indeed, the CNN monomer possesses only a shallow saucer-like  
395 shape with a small concave at the center, confirmed by X-ray crystallographic analysis (Bradbrook  
396 et al., 2000, Yang et al., 2012). Considering this CNN architecture, the doxorubicin might be mainly  
397 entrapped in the hydrophilic nanochannels of the polymer network. The drug loading was 15.5% for  
398 doxorubicin-loaded CNN-NS (1:4), with an encapsulation efficiency of about 95%.  
399 Figure 3 shows the SEM (A) and TEM (B) images of CNN-NS before and after HPH step  
400 respectively.



401  
402

403 **Figure 3.** A) SEM image of CNN-NS before HPH step and B) TEM image of the CNN-NS after  
404 HPH step (TEM scale bar 300 nm).

405

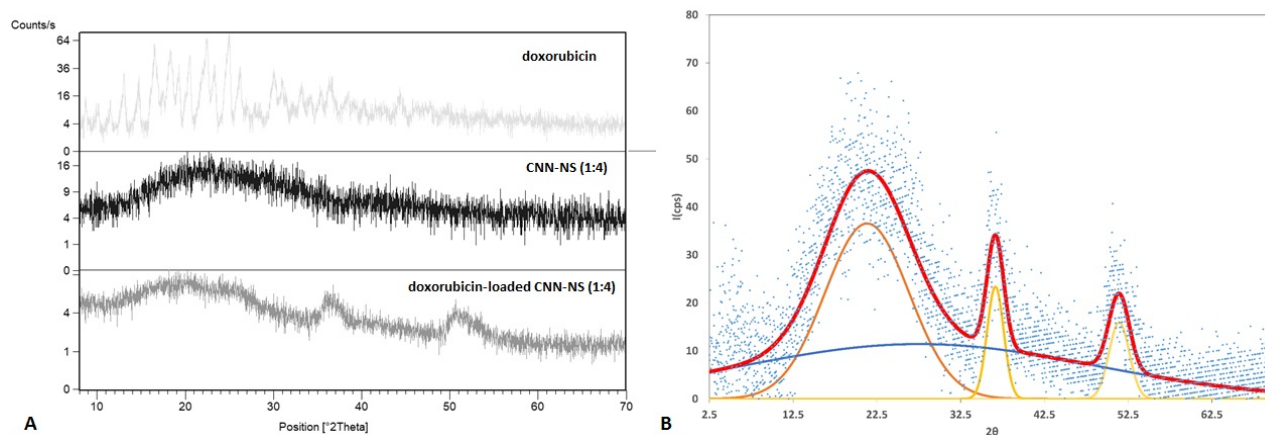
406 Figure 3A shows the irregular morphology and large particle size of NS prior to HPH treatment.  
407 As reported in the literature (Trotta, 2011), dextrin-based NS have generally rather compact  
408 structures. Also in the case of CNN-NS, BET analysis revealed surface area values below 2 m<sup>2</sup>/g  
409 (data not shown). Cyclodextrin- and CNN-NS have nanometric and sub-nanometric intrinsic  
410 porosity, deriving from the inner cavities of dextrin monomers and from the interstitial volumes  
411 among dextrin monomers. Such molecular-level porosity cannot be discerned by means of scanning  
412 electron microscopy. TEM image (Fig. 3B) shows the CNN-NS spherical shape and confirms the  
413 nanoscaled sizes, reached after the homogenization process.

414 When loaded with doxorubicin, CNN-NS lose their frankly amorphous behaviour, increasing their  
415 low range ordering. Indeed, the new order does not tally with the structure of crystalline  
416 doxorubicin, as shown in Figure 4A. The presence of a few broad diffraction peaks in the  
417 diffraction pattern of the loaded CNN-NS demonstrates the formation of a brand new, poorly

418 ordered phase; that ordering is presumably due to the inkling ordering of the doxorubicin inside the  
 419 nanosponge.

420

421



422

423 **Figure 4.** A) CNN-NS (1:4) loading with doxorubicin leads to a deep modification of the  
 424 nanosponge diffraction pattern (doxorubicin-loaded CNN-NS (1:4) in figure) B) Experimental data  
 425 (dots) and calculated function (red curve) of XRPD of the doxorubicin-loaded CNN-NS. Broad  
 426 yellow curves represent the decomposition of the XRPD pattern, while the blue one corresponds to  
 427 the amorphous background.

428

429 **Table 4:** Position, height, area and full width at half maximum of the three diffraction peaks of the  
 430 CNN 1:4 loaded with doxorubicin

431

#	Center (°2θ)	Height (cps)	Area (cps)	FWHM (°2θ)
1	21.3426	37.5097	478.982	11.9962
2	36.6454	23.6005	60.563	2.41077
3	51.4022	16.0661	48.7831	2.85251

432

433

434

435

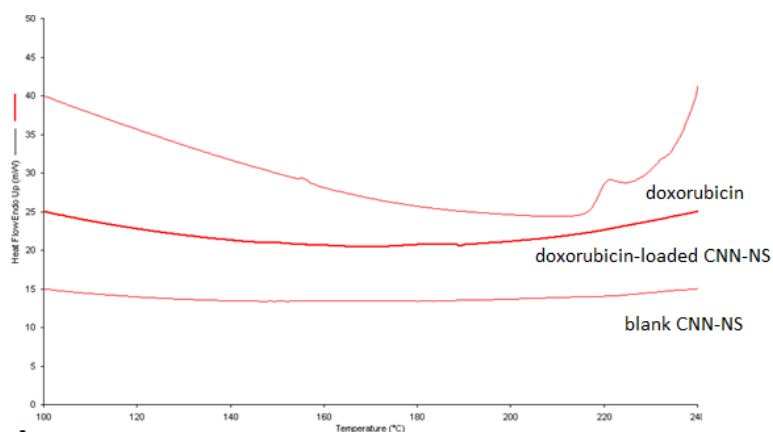
436 The diffraction data of the CNN 1:4 nanosponges with doxorubicin were decomposed using the  
437 Fityk software (Wojdyr, 2010). The decomposition of the XRPD pattern shows at least three curves  
438 representing the poor ordering of the system.

439 Due to the broad behaviour of the peaks, a Gaussian profile fitting was selected. The pattern shows  
440 a bump (blue line in Figure 4B) ascribable to the amorphous phase and three broad peaks (yellow)  
441 possibly related to the weak ordering of the doxorubicin in the loaded nanosponge.

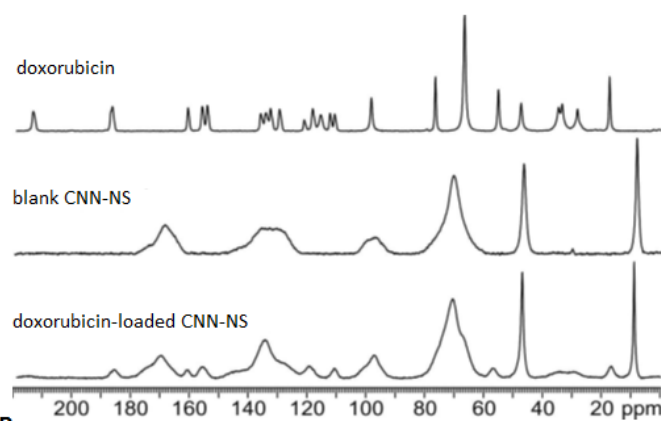
442 DSC analysis of doxorubicin-loaded CNN-NS showed the drug incorporation in the nanosponge  
443 matrix (Figure 5A). Indeed, the endothermic peak related to the melting of doxorubicin at about  
444 220°C is missing in the thermograms of doxorubicin-loaded CNN-NS, indicating that the drug is  
445 molecularly dispersed in the polymer matrix.

446 The cross-linked structure of CNN-NS was confirmed by <sup>13</sup>C solid state NMR analysis. Signals  
447 deriving from carbonyl groups in ester/carboxylic moieties and aromatic carbon atoms belonging to  
448 PMDA units appear at approximately 170 and 130 ppm, respectively (figure 5B).

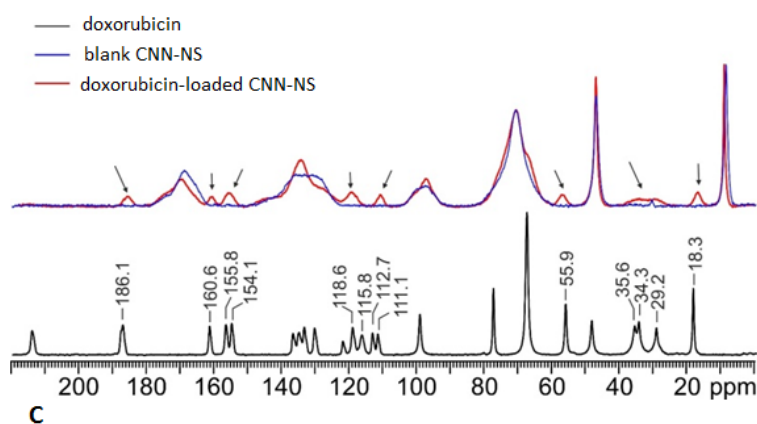
449 In addition, solid state NMR confirmed the interaction of the drug with CNN-NS.



**A**



**B**



**C**

450

451 **Figure 5. A)** DSC thermograms of CNN-NS (1:4), free doxorubicin and doxorubicin-loaded CNN-

452 NS **B)** Solid NMR profiles of CNN-NS (1:4), free doxorubicin and CNN-NS. **C)** Comparison

453 between  $^{13}\text{C}$  CPMAS spectra of doxorubicin, blank nanosponge and doxorubicin-loaded CNN-NS

454 in the 0-220 ppm range. Arrows and chemical shift values facilitate the identification of significant

455 peaks.

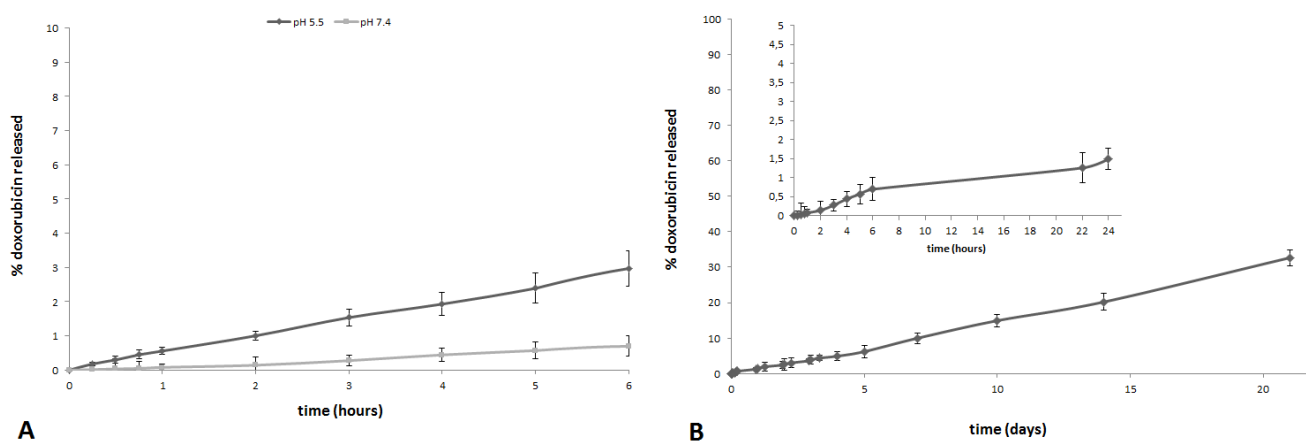
456

457

458 Figure 5b shows the  $^{13}\text{C}$  CPMAS SSNMR spectra of doxorubicin, blank CNN-NS (1:4) and  
459 doxorubicin-loaded CNN-NS (1:4). Figure 5c shows the comparison between the spectra of the  
460 three samples. In the spectrum of the loaded sample (doxorubicin-loaded CNN-NS, red) several  
461 signals, different from the characteristic peaks of the CNN-NS (blank nanosponges, blue), are  
462 observed and indicated with arrows. These signals are compliant with the typical chemical shifts of  
463 the  $^{13}\text{C}$  atoms of doxorubicin (also shown in the figure) and thus evidence the presence of  
464 doxorubicin inside the nanosponges.

465 Then, the *in vitro* doxorubicin release kinetics from CNN-NS was evaluated at pH 5.5 and at pH 7.4  
466 (Figure 6A).

467



468

469

470 **Figure 6. A)** *In vitro* release kinetics of doxorubicin from CNN-NS (1:4) as a function of pH; **B)** *In*  
471 *vitro* release kinetics of doxorubicin from CNN-NS (1:4) at pH = 7.4

472

473 *In vitro* release profiles showed a very slow and constant release of the drug over time depending on  
474 the pH value of the receiving phase. Interestingly, no burst effect was observed at both pH values.  
475 After 24 hours only 1.3% of doxorubicin was released from CNN-NS at pH 7.4, while the  
476 percentage of doxorubicin released at pH 5.5 reached 10%. The slow and pH-sensitive release  
477 profile may be related to the chemical structure of CNN-NS. The main role is played by the  
478 polymer matrix, which comprises free carboxylic groups in the polymer network. The carboxylic  
479 groups, belonging from the pyromellitic dianhydride used as cross-linker, are only partially  
480 dissociated at pH 5.5 resulting in lower interactions and favouring the drug release. On the other  
481 hand, the cavity of CNN monomer is not suitable for doxorubicin complexation being a very small  
482 pocket, as previously reported. Considering the  $\beta$ -cyclodextrin-based NS obtained by reacting  $\beta$ -CD

483 with pyromellitic dianhydride, a doxorubicin release of about 10% was reached after 6 hours at pH  
484 7.4 (data not shown). This different behaviour might be related to the narrow polymer meshes  
485 present in CNN-NS. Indeed, the extremely slow and prolonged release behaviour from CNN-NS  
486 compared to other doxorubicin nanosponge formulations at pH 7.4 (Cavalli, Trotta & Tumiatti,  
487 2006) might represent an advantage to limit the drug blood exposure and the toxicity of  
488 doxorubicin.

489 We speculate that doxorubicin may be released in a controlled manner following Fickian kinetics  
490 due to drug diffusion through the polymeric matrix, which underwent degradation with a very slow  
491 kinetics due to hydrolysis. Indeed, the absence of any burst effect could indicate that doxorubicin is  
492 not adsorbed on the nanosponge surface and CNN-NS are slowly degraded in the physiological  
493 environment.

494 The release mechanism was further evaluated. The doxorubicin *in vitro* release from drug-loaded  
495 CNN-NS was fitted to four distinct models to determine which one exhibited the highest correlation  
496 with the experimental results. For each model, the rate constant and correlation values were  
497 obtained by applying a linear regression fit. The zero-order kinetic model demonstrated the higher  
498 correlation, showing  $R^2$  values of 0.9969 and 0.9985 for doxorubicin release at pH 7.4 and pH 5.5,  
499 respectively.

500 The *in vitro* release kinetics of doxorubicin from CNN-NS at pH 7.4 was followed up to 21 days  
501 (Figure 6B).

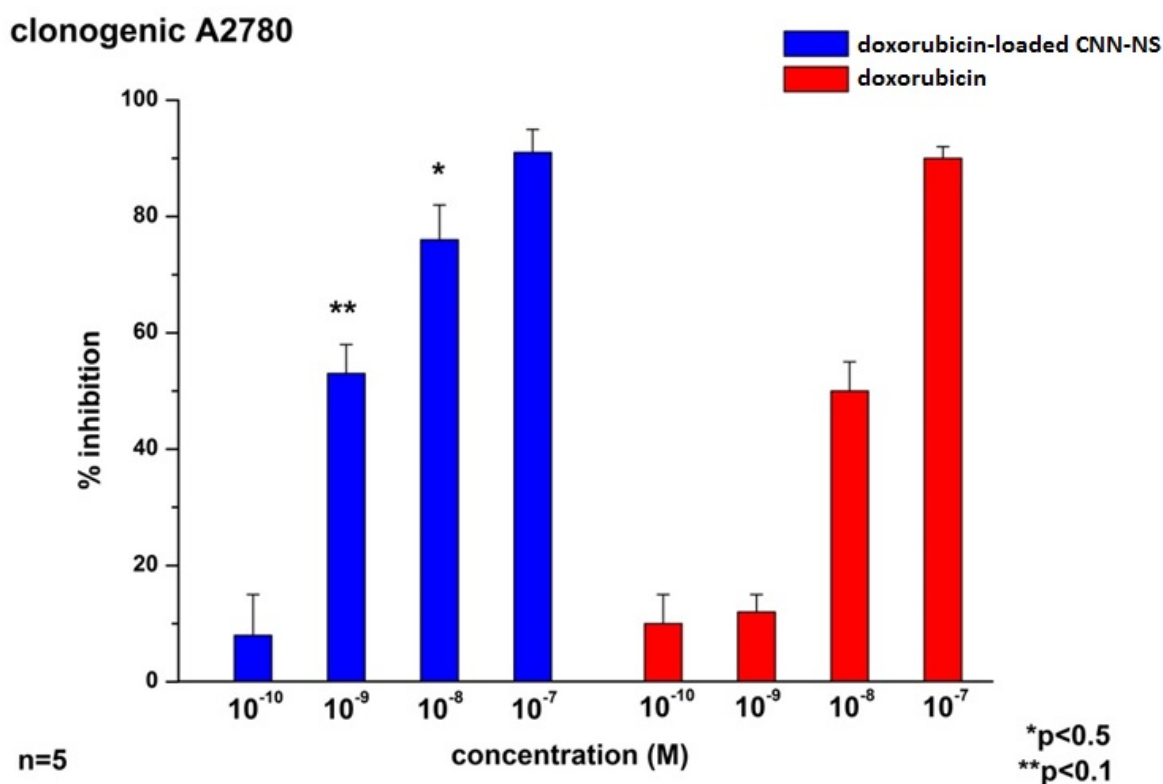
502 Intriguingly, the results indicate that at physiological pH value, CNN-NS provide a slow drug  
503 diffusion and controlled release over a lengthy period. Indeed, after 14 days at pH 7.4 only about  
504 20% of the drug was released and after 21 days this reached about 32.5%. This behaviour could be  
505 exploited to obtain a constant drug concentration in tumour tissue in loco-regional treatment (Cheng  
506 et al., 2017, Cinar et al., 2017). Interestingly, the tumour environment pH is more acid than that of  
507 normal tissue (Manchun, Dass & Sriamornsak, 2012).

508 In order to verify the absence of nanosponge activity, cells were treated with plain CNN-NS at  
509 dilutions corresponding to that drug-loaded CNN-NS. In all the concentrations tested, the results  
510 overlapped with those obtained in controls, with no significant inhibition of cell proliferation, thus  
511 excluding any toxic effect of the nanocarriers.

512 Concerning CNN-NS safety, no significant hemolysis caused by CNN-NS either blank or  
513 doxorubicin loaded was observed, confirming their good biocompatibility and the presence of  
514 tonicity values suitable for a future potential *in vivo* administration.

515 Clonogenic survival assays were performed. The cells were seeded 6-well plates and treated with  
516 each compound. The culture medium was changed after 72 h, and the cells were cultured for an  
517 additional 10 days in the absence of the compounds. The results showed that doxorubicin or CNN  
518 doxorubicin treatments differently inhibited the ability of the A2780 cell line to form colonies. In  
519 fact, both formulations induced the maximum effect at  $10^{-7}$ M, but doxorubicin-loaded CNN-NS  
520 were able to induce a higher inhibition of the colony formation at  $10^{-8}$ - $10^{-9}$ M, determining growth  
521 inhibition around 80% and 50%, respectively. Conversely, the treatment with doxorubicin in  
522 solution produced a smaller inhibition of the ability to form colonies (50%) at  $10^{-8}$  M, being no  
523 more active at the lower concentration.

524  
525



526

527 **Figure 7.** Effect of doxorubicin and doxorubicin-loaded CNN-NS on cell clonogenicity was tested  
528 by colony forming assay. A2780 cells (1000 per well) were seeded in six-well plates and treated  
529 with each drug at the indicated concentrations for 72 h. The medium was then changed and cells  
530 were cultured for additional 10 days and subsequently fixed and stained with crystal violet. Data  
531 shown are means  $\pm$ SEM ( $n = 5$ ).  $**P < 0.01$ ,  $*P < 0.05$  significantly different from the same  
532 concentration of doxorubicin.

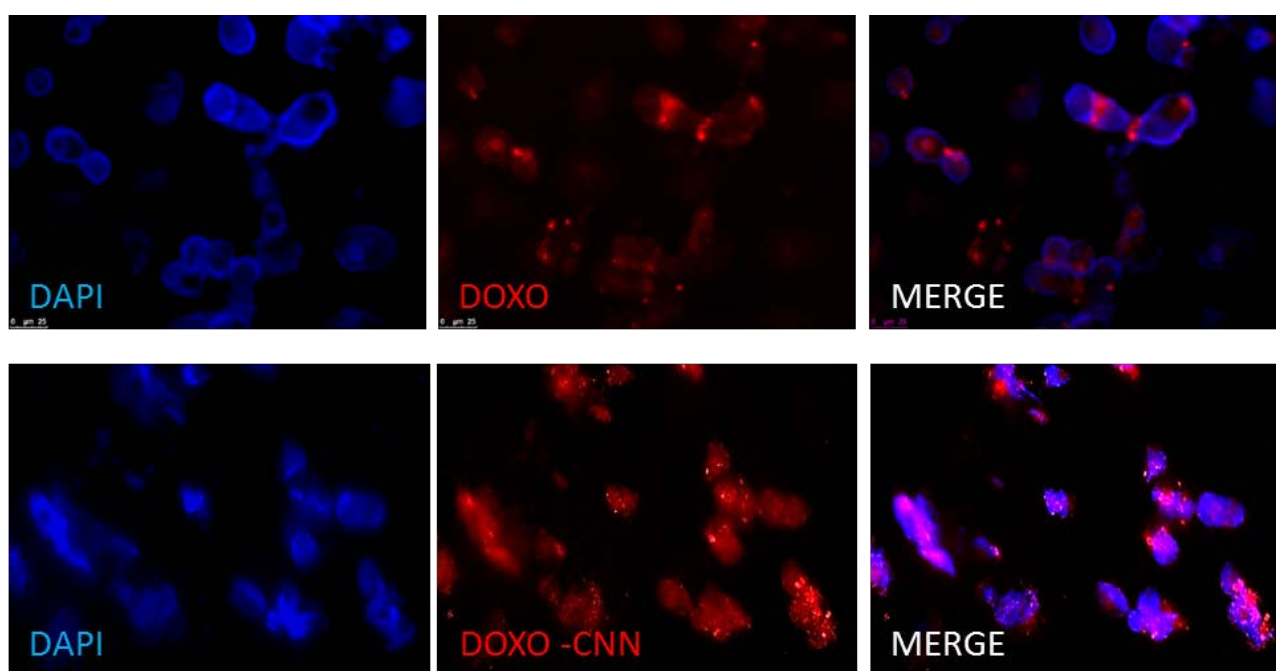
533



534 Indeed, the  $IC_{50}$  was  $0.9 \pm 0.2 \times 10^{-9} M$  and  $8.5 \pm 1 \times 10^{-9} M$ , respectively for doxorubicin-loaded  
535 CNN-NS and for free doxorubicin. Therefore, the cytotoxicity of doxorubicin loaded in  
536 nanosponges was enhanced of about 8 fold than free drug on A2780 cell lines.

537 Cell uptake is promoted by nanocarriers as previously shown with various nanoformulations  
538 (Miglietta, Cavalli, Bocca, Gabriel & Gasco, 2000, Ernsting, Murakami, Roy, & Li, 2013, Wang et  
539 al., 2016). The size, surface charge and the components of CNN-NS might favored the cell  
540 internalization. Indeed, *in vitro* uptake results demonstrated that fluorescence was localized in the  
541 cytoplasm around the nucleus to a greater extent in the cells treated with doxorubicin-loaded CNN-  
542 NS, indicating that CNN-NS had been internalised in a greater extent into the cells.

543



544

545 **Figure 8.** Cell uptake was evaluated by fluorescence microscopy analysis using different doses of  
546 doxorubicin-loaded CNN-NS (DOXO-CNN) o free DOX on A2780 cells for 48 h.

547

548 Clonogenic assay or colony formation assay is an *in vitro* cell survival assay based on the ability of  
549 a single cell to grow into a colony. Only a fraction of seeded cells retains the capacity to produce  
550 colonies. After plating at very low density (800 cells for wells), cells are treated with the  
551 compounds for 72h, thus they were washed with the cell medium, to remove drugs, and were then  
552 allowed to grow over an extended period of time (10 days). Doxorubicin-loaded CNN-NS may act  
553 as intracellular drug reservoir slowly releasing the free drug into the cellular cytoplasm, enhancing  
554 its therapeutic efficacy. Doxorubicin encapsulation in CNN-NS might increase its concentration at

555 the tumor site, thereby decreasing the frequent dose administered and subsequently reducing the  
556 side effects. In this *in vitro* assay, free DOX is also able to inhibit the colony formation, especially  
557 at the highest concentration tested ( $10^{-7}$ M), considering the static conditions of the experimental set-  
558 up. We can hypothesize a different behaviour *in vivo*. Various factors controlled the  
559 pharmacokinetics, biodistribution and intratumoral penetration of nanoparticles after their *in vivo*  
560 administration (Ernsting et al., 2013). A crucial role is played by the EPR effect, that allows the  
561 nanoparticles to escape from the vessels and enter in the tumor cells.

562

#### 563 **4. Conclusions**

564 A new polymer-based nanomaterial was obtained, exploiting a tetraglucose, i.e. CNN, as a  
565 monomer in the synthetic reaction. The cross-linking reaction with pyromellitic dianhydride formed  
566 solid nanoparticles, named nanosponges. This new nanomaterial is biocompatible and is able to  
567 swell in response to the pH value. CNN-NS can be formulated as nanoscale particles with spherical  
568 shape suitable for drug delivery. Doxorubicin was incorporated in a good extent and released with a  
569 very slow and constant kinetics. Interestingly, the environment pH play a role in controlling the  
570 release profile of the drug.

571 Based on the results, doxorubicin-loaded CNN-NS might act as a nanomedicine tool for tumor local  
572 treatment with a favorable toxicology profile.

573

#### 574 **Acknowledgements**

575 R. Cavalli and C Dianzani was funded by University of Turin (ex-60 %) funds.

576 The authors thanks prof. Roberto Gobetto and Ms. Federica Rossi for SS-NMR analyses.

577

#### 578 **Author contribution**

579 FC synthesized the CNN-nanosponges, MA and MT formulated and *in vitro* characterized the  
580 nanoformulations, LG and CD performed cell culture experiments, LP and DA performed XRPD  
581 analyses, FT and RC designed the experiments and gave the intellectual rationale to the work, TN  
582 and TH samples gift and chemical information on cyclic nigerosyl-1-6-nigerose.

583

584 **References**

- 585 • Aga, H., Nishimoto, T., Kuniyoshi, M., Maruta, K., Yamashita, H., Higashiyama, T.,  
586 Nakada, T., Kubota, M., Fukuda, S., Kurimoto, M., Tsujisaka, Y. (2003). 6- $\alpha$ -  
587 Glucosyltransferase and 3- $\alpha$ -Isomaltosyltransferase from *Bacillus globisporus* N75. *Journal*  
588 *of Bioscience and Bioengineering*, 95(3), 215-224.
- 589 • Arpicco, S., Battaglia, L., Brusa, P., Cavalli, R., Chirio, D., Dosio, F., Gallarate, M., Milla,  
590 P., Peira, E., Rocco, F., Sapino, S., Stella, B., Ugazio, E., Ceruti, M. (2016). Recent studies  
591 on the delivery of hydrophilic drugs in nanoparticulate systems. *Journal of Drug Delivery*  
592 *Science and Technology*, 32, 298-312.
- 593 • Bastiancich, C., Scutera, S., Alotto, D., Cambieri, I., Fumagalli, M., Casarin, S., Rossi, S.,  
594 Trotta, F., Stella, M., Cavalli, R., Musso, T., Castagnoli, C. (2014). Cyclodextrin-Based  
595 Nanosponges as a Nanotechnology Strategy for Imiquimod Delivery in Pathological  
596 Scarring Prevention and Treatment. *Journal of Nanopharmaceutics and Drug Delivery*,  
597 2(4), 311-324.
- 598 • Bhattacharjee, S., Sarkar, B., Sharma, A.R., Gupta, P., Sharma, G., Lee, S.S., Chakraborty,  
599 C. (2016). Formulation and Application of Biodegradable Nanoparticles Based  
600 Biopharmaceutical Delivery - An Efficient Delivery System. *Curr Pharm Des.* 22(20),3020-  
601 3033.
- 602 • Bradbrook, GM., Gessler, K., Cote, GL., Momany, F., Biely, P., Bordet, P., Perez, S.,  
603 Imberty ,A. (2000). X-ray structure determination and modeling of the cyclic  
604 tetrasaccharidecyclo-( $\rightarrow$ 6)- $\alpha$ -D-Glcp-(1 $\rightarrow$ 3)- $\alpha$ -D-Glcp- {1 $\rightarrow$ 6)- $\alpha$ -D-Glcp-(1 $\rightarrow$ 3)- $\alpha$ -Glcp-  
605 (1 $\rightarrow$ }. *Carbohydr Res.*329, 655–665.
- 606 • Brigger, I., Dubernet, C., Couvreur, P. (2002). Nanoparticles in cancer therapy and  
607 diagnosis. *Advanced Drug Delivery Reviews*, 54(5), 631-651.
- 608 • Cavalli, R., Ansari, A.K., Bisazza, A., Giustetto, P., Trotta, F., Vavia, P.R. (2010).  
609 Nanosponge formulations as oxygen delivery systems. *Internation Journal of*  
610 *Pharmaceutics*, 402, 254-257.
- 611 • Caldera, F., Tannous, M., Cavalli, R., Zanetti, M.,Trotta, F. (2017). Evolution of  
612 cyclodextrin nanosponges. *International journal of pharmaceutics*, 531(2), 470-479.
- 613 • Cavalli, R., Trotta, F.,Tumiatti, W. (2006). Cyclodextrin-based nanosponges for drug  
614 delivery. *Journal of inclusion phenomena and macrocyclic chemistry*, 56(1-2), 209-213.

- 615 • Cheng, R., Meng, F., Deng, C., Klok, H.A., Zhong, Z. (2013). Dual and multi-stimuli  
616 responsive polymeric nanoparticles for programmed site-specific drug delivery.  
617 *Biomaterials*, 34(14), 3647-3657.
- 618 • Cheng, W., Nie, J., Xu, L., Liang, C., Peng, Y., Liu, G., Wang, T., Mei, L., Huang, L., Zeng,  
619 X. (2017). pH-Sensitive Delivery Vehicle Based on Folic Acid-Conjugated Polydopamine-  
620 Modified mesoporous Silica Nanoparticles for Targeted Cancer Therapy. *ACS Applied*  
621 *Material and Interfaces*, 9(22), 18462-18473.
- 622 • Cinar, G., Ozdemir, A., Hamsici, S., Gunay, G., Dana, A., Tekinay A.B., Guler, M.O.  
623 (2017). Local delivery of doxorubicin through supramolecular peptide amphiphile nanofiber  
624 gels. *Biomaterial Science*, 5, 67–76.
- 625 • Daga, M., Ullio, C., Argenziano, M., Dianzani, C., Cavalli, R., Trotta, F., Ferretti, C., Zara,  
626 G.P., Gigliotti, C.L., Ciamporzero, E.S., Pettazzoni, P., Corti, D., Pizzimenti, S. (2016).  
627 GSH-targeted nanosponges increase doxorubicin-induced toxicity "in vitro" and "in vivo" in  
628 cancer cells with high antioxidant defenses. *Free Radical Biology and Medicine*, 97, 24-37.
- 629 • Dinarvand, R., Sepehri, N., Manoochehri, S., Rouhani, H., Atyabi F. (2011). Polylactide-co-  
630 glycolide nanoparticles for controlled delivery of anticancer agents. *International Journal of*  
631 *Nanomedicine*, 6, 877-95.
- 632 • Duchene, D., Cavalli, R., Gref, R. (2016). Cyclodextrin-based polymeric nanoparticles as  
633 efficient carriers for anticancer drugs. *Current pharmaceutical biotechnology*, 17(3), 248-  
634 255.
- 635 • Ernsting, M.J., Murakami, M., Roy, A., & Li, S. D. (2013). Factors controlling the  
636 pharmacokinetics, biodistribution and intratumoral penetration of nanoparticles. *Journal of*  
637 *controlled release*, 172(3), 782-794.
- 638 • Fang, J., Nakamura, H., Maeda, H. (2011). The EPR effect: Unique features of tumor blood  
639 vessels for drug delivery, factors involved, and limitations and augmentation of the effect.  
640 *Advanced Drug Delivery Reviews*, 63(3), 136-15.
- 641 • Gigliotti, C.L., Ferrara, B., Occhipinti, S., Boggio, E., Barrera, G., Pizzimenti, S.,  
642 Giovarelli, M., Fantozzi, R., Chiochetti, A., Argenziano, M., Clemente, N., Trotta, F.,  
643 Marchiò, C., Annaratone, L., Boldorini, R., Dianzani, U., Cavalli, R., Dianzani C. (2017).  
644 Enhanced cytotoxic effect of camptothecin nanosponges in anaplastic thyroid cancer cells in  
645 vitro and in vivo on orthotopic xenograft tumors. *Drug Delivery*, 24(1), 670-680.

- 646 • Hamidi, M., Azadi, A., Rafiei, P., Ashrafi, H. (2013). A pharmacokinetic overview of  
647 nanotechnology-based drug delivery systems: an ADME-oriented approach. *Crit Rev Ther*  
648 *Drug Carrier Syst.* 30(5), 435-67.
- 649 • Ishikawa, H., Kuwano, H., Chaen, H., Matsumoto, K. (2009). Complexation of Some  
650 Aromatic Compounds with Cyclic Nigerosyl-(1→ 6)-Nigerose. *Journal of Faculty of*  
651 *Agriculture, Kyushu University*, 54(1), 201-204.
- 652 • Jaimes-Aguirre, L., Gibbens-Bandala, B.V., Morales-Avila, E., Ocampo-García, B.E.,  
653 Seyedeh-Fatemeh, M., Amirhosein, A. (2016). Polymer-Based Drug Delivery Systems,  
654 Development and Pre-Clinical Status. *Curr Pharm Des.* 22(19), 2886-903.
- 655 • Jaimes-Aguirre, L., Morales-Avila, E., Ocampo-García, B.E., Medina, L.A., López-Téllez,  
656 G., Gibbens-Bandala, B.V., Izquierdo-Sánchez, V. (2017). Biodegradable poly(D,L-lactide-  
657 co-glycolide)/poly(L- $\gamma$ -glutamic acid) nanoparticles conjugated to folic acid for targeted  
658 delivery of doxorubicin. *Materials Science and Engineering C, Materials for Biological*  
659 *Applications*, 76, 743-751.
- 660 • Khan, I., Gothwal, A., Sharma, A.K., Kesharwani, P., Gupta, L., Iyer, A.K., Gupta U.  
661 (2016). PLGA Nanoparticles and Their Versatile Role in Anticancer Drug Delivery.  
662 *Critical Reviews in Therapeutic Drug Carrier Systems*, 33(2), 159-93.
- 663 • Lembo, D., Swaminathan, S., Donalisio, M., Civra, A., Pastero, L., Aquilano, D., Vavia, P.,  
664 Trotta, F., Cavalli R. (2013). Encapsulation of Acyclovir in new carboxylated cyclodextrin-  
665 based nanosponges improves the agent's antiviral efficacy. *International Journal of*  
666 *Pharmaceutics*, 443(1-2), 262-72.
- 667 • Liang, W., Yang, C., Zhou, D., Haneoka, H., Nishijima, M., Fukuhara, G., Mori, T.,  
668 Catiglione F., Mele, A., Caldera, F., Trotta, F., Inoue, Y. (2013). Phase-controlled  
669 supramolecular photochirogenesis in cyclodextrin nanosponges. *Chemical Communications*,  
670 49(34), 3510-3512.
- 671 • Liang, W., Zhao, M., Wei, X., Yan, Z., Wu, W., Caldera, F., Trotta, F., Inoue, Y., Su, D.,  
672 Zhong, Z., Yang, C. (2017). Photochirogenic nanosponges: phase-controlled  
673 enantiodifferentiating photoisomerization of (Z)-cyclooctene sensitized by pyromellitate-  
674 crosslinked linear maltodextrin. *RSC Advances*, 7(28), 17184-17192.
- 675 • Liu, X., Yang, Y., Urban, M.W. (2017). Stimuli-Responsive Polymeric Nanoparticles.  
676 *Macromol Rapid Commun.* 38(13).

- 677 • Maeda, H., Nakamura, H., Fang, J. (2013). The EPR effect for macromolecular drug  
678 delivery to solid tumors: Improvement of tumor uptake, lowering of systemic toxicity, and  
679 distinct tumor imaging in vivo. *Advanced Drug Delivery Reviews*, 65(1), 71-79.
- 680 • Manchun, S., Dass, C.R., Sriamornsak, P. (2012). Targeted therapy for cancer using pH-  
681 responsive nanocarrier systems. *Life Sciences*, 90(11-12), 381-387.
- 682 • Miglietta, A., Cavalli, R., Bocca, C., Gabriel, L., Gasco, M.R. (2000). Cellular uptake and  
683 cytotoxicity of solid lipid nanospheres (SLN) incorporating doxorubicin or paclitaxel.  
684 *International Journal of Pharmaceutics*, 210(1), 61-67.
- 685 • Muankaew, C., & Loftsson, T. (2018). Cyclodextrins-based Formulations: A Non-Invasive  
686 Platform for Targeted Drug Delivery. *Basic & clinical pharmacology & toxicology*, 122, 46-  
687 55..
- 688 • Mura, S., Nicolas, J., Couvreur, P. (2013). Stimuli-responsive nanocarriers for drug delivery.  
689 *Nature materials*, 12(11), 991-1003.
- 690 • Natarajan, J.V., Nugraha, C., Ng, X.W., Venkatraman, S. (2014). Sustained-release from  
691 nanocarriers: a review. *Journal of Controlled Release*, 193, 122-138.
- 692 • Nishimoto, T., Aga, H., Mukai, K., Hashimoto, T., Watanabe, H., Kubota, M., Fukuda, S.  
693 Kurimoto, M., Tsujisaka, Y. (2002). Purification and Characterization of  
694 Glucosyltransferase and Glucanotransferase Involved in the Production of Cyclic  
695 Tetrasaccharide in *Bacillus globisporus* C11. *Bioscience. Biotechnology. Biochemistry*,  
696 66(9), 1806-1818.
- 697 • Oku, K., Kudou, N., Kurose, M., Shibuya, T., Chaen, H., Fukuda, S. (2007). The crystal  
698 properties of cyclic nigerosyl-(1-6)-nigerose (CNN) and powdering of alpha-tocopherol,  
699 cholecalciferol and EPA using CNN. *Journal of the Japanese Society for Food Science and  
700 Technology (Japan)*.
- 701 • Prasad, M., Lambe, U. P., Brar, B., Shah, I., Manimegalai, J., Ranjan, K., Rao, R. Kumar, S.,  
702 Mahant, S., Khurana, S.K., Iqbal, H.M., Dhama, K., Misri, J., Prasad, G. (2018).  
703 Nanotherapeutics: An insight into healthcare and multi-dimensional applications in medical  
704 sector of the modern world. *Biomedicine & Pharmacotherapy*, 97, 1521-1537.
- 705 • Sherje, A. P., Dravyakar, B. R., Kadam, D., & Jadhav, M. (2017). Cyclodextrin-based  
706 nanosponges: a critical review. *Carbohydrate polymers*, 173, 37-49.
- 707 • Swaminathan, S., Cavalli, R., Trotta, F., Ferruti, P., Ranucci, E., Gerges, I., Manfredi, A.,  
708 Marinotto, D., Vavia P.R. (2010a). In vitro release modulation and conformational

- 709 stabilization of a model protein using swellable polyamidoamine nanosponges of  $\beta$ -  
710 cyclodextrin. *Journal of Inclusion Phenomena and Macrocyclic Chemistry*, 68(1-2), 183-  
711 191.
- 712 • Swaminathan, S., Pastero, L., Serpe, L., Trotta, F., Vavia, P., Aquilano, D., Trotta, M., Zara,  
713 G.P., Cavalli, R. (2010b). Cyclodextrin-based nanosponges encapsulating camptothecin:  
714 physicochemical characterization, stability and cytotoxicity. *European Journal of*  
715 *Pharmaceutics and Biopharmaceutics*, 74, 193-201.
  - 716 • Torne, S., Ansari, K., Vavia, P.R., Trotta, F., Cavalli, R. (2010). Enhanced oral paclitaxel  
717 bioavailability after administration of paclitaxel-loaded nanosponges. *Drug Delivery*, 17(6),  
718 419-425.
  - 719 • Trotta, F. (2011). Cyclodextrin Nanosponges and Their Applications. *Cyclodextrins in*  
720 *Pharmaceutics, Cosmetics, and Biomedicine*, Wiley, Hoboken.
  - 721 • Trotta, F., Zanetti, M., Cavalli, R. (2012). Cyclodextrin-based nanosponges as drug carriers.  
722 *Beilstein Journal of Organic Chemistry*, 8, 2091-2099.
  - 723 • Trotta, F., Dianzani, C., Caldera, F., Mognetti, B., Cavalli, R. (2014). The application of  
724 nanosponges to cancer drug delivery. *Expert Opinion on Drug Delivery*, 11(6), 931-941.
  - 725 • Wang, H. X., Zuo, Z. Q., Du, J. Z., Wang, Y. C., Sun, R., Cao, Z. T., Ye, X., Wang, J.,  
726 Leong, K.W., Wang, J. (2016). Surface charge critically affects tumor penetration and  
727 therapeutic efficacy of cancer nanomedicines. *Nano Today*, 11(2), 133-144.
  - 728 • Watanabe, H., Nakano, M., Oku, K., Aga, H., Nishimoto, T., Kubota, M., Fukuda, S.,  
729 Kurimoto, M., and Tsujisaka Y. (2004). Cyclic tetrasaccharides in sake lees. *J. Appl.*  
730 *Glycosci.* 51, 345-347
  - 731 • Wei, X., Liang, W., Wu, W., Yang, C., Trotta, F., Caldera, F., Mele, A., Nishimoto, T.,  
732 Inoue, Y. (2015). Solvent- and phase-controlled photochirogenesis. Enantiodifferentiating  
733 photoisomerization of (Z)-cyclooctene sensitized by cyclic nigerosyl-nigerose-based  
734 nanosponges crosslinked by pyromellitate. *Organic & biomolecular chemistry*, 13(10),  
735 2905-2912.
  - 736 • Weissenfeld, M. (2005). Hydrolysis determination of CT-11 at different pH values.  
737 Unpublished study report of RCC Ltd. for Hayashibara International, Inc., Westminster,  
738 USA. 11 March, 2005.
  - 739 • Wojdyr, M.J. (2010). Fityk: a general-purpose peak fitting program. *Journal of Applied*  
740 *Crystallography*, 4(5), 1126-1128

- 741 • Yang, C., Liang, W., Nishijima, M., Fukuhara, G., Mori, T., Hiramatsu, H., ... & Inoue, Y.  
742 (2012). Supramolecular Photochirogenesis with Novel Cyclic Tetrasaccharide:  
743 Enantiodifferentiating Photoisomerization of (Z)-Cyclooctene with Cyclic  
744 Nigerosylnigerose-Based Sensitizers. *Chirality*, 24(11), 921-927  
745